Appl. Phys. B 81, 607–613 (2005)
DOI: 10.1007/s00340-005-1916-0

Applied Physics B
Lasers and Optics

D.F.P. PILE✉

Compact-2D FDTD for waveguides including materials with negative dielectric permittivity, magnetic permeability and refractive index

Department of Optical Science and Technology, Faculty of Engineering, The University of Tokushima, Minamijosanjima 2-1, Tokushima 770-8506, Japan
Applied Optics Program, School of Physical and Chemical Sciences, Queensland University of Technology, GPO Box 2434, Brisbane, QLD 4001, Australia

Received: 19 March 2005 / Revised version: 28 May 2005
Published online: 19 July 2005 •

ABSTRACT An efficient compact-2D finite-difference time-domain method is presented for the numerical analysis of guided modes in waveguides that may include negative dielectric permittivity, negative magnetic permeability and negative refractive index materials. Both complex variable and real variable methods are given. The method is demonstrated for the analysis of channel-plasmon-polariton guided modes in triangular groves on a metal surface. The presented method can be used for a range of waveguide problems that were previously unsolvable analytically, due to complex geometries, or numerically, due to computational requirements of conventional three-dimensional finite-difference time-domain methods. A three-dimensional finite-difference time-domain algorithm that also allows analysis in the presence of bound or free electric and equivalent magnetic charges is presented and an example negative refraction demonstrates the method.

PACS 02.70.Bf; 47.79.Gn; 02.60.Cb

1 Introduction

One of the most powerful methods for the analysis of electromagnetic problems is the numerical solution of Maxwell's equations by the finite-difference time-domain (FDTD) method [1, 2]. However, the computational resources required prohibits the analysis of many structures, particularly if they require three-dimensional (3D) analysis. At the same time, conventional FDTD [1] can not be used for modeling materials that exhibit negative dielectric permittivity (metals below the plasma frequency or conventional dielectric at a frequency near a material resonance, etc.), magnetic permeability (magnetic materials) at the frequency (frequencies) of consideration [3, 4]. This is because of positive feedback in the time-domain algorithm when attempting to model frequency-domain parameters resulting in unphysical rapid increase of the fields in the computation window, i.e., numerical instability. Naturally this includes materials with negative refractive index (simultaneous negative dielectric permittivity and magnetic permeability) that were theoretically proposed almost 40 years ago [5] but have been receiving a lot of attention in recent years since they were experimentally verified in the microwave regime [6] (though different metamaterials or photonics crystals may allow observation of negative refraction at higher frequencies (e.g., near-infrared and optical frequencies [7]). In recent years, conventional FDTD was extended for the analysis of dielectrics at a frequency near an electronic resonance (where the dielectric permittivity can be negative) using a bound electron model and also for also for metals using a free electron model (or bound electron model when operating above the plasma frequency) [3, 4]. Later the conventional FDTD method was extended to allow for materials that exhibit negative refractive index materials [8].

It has been shown that the computational requirements for the analysis of guided modes in dielectric structures can be drastically reduced by assuming translational symmetry of the structure along the direction of propagation. In this case the field components have a known dependence of the form, $\exp(ikz)$, along this axis (where k is the wave number of the guided mode). This method was named compact-2D FDTD [9–11] and was previously used for analysis of guided modes in conventional anisotropic dielectric waveguides [9] as well as photonic crystal fibres [11].

At the same time, miniaturization of optical dielectric waveguides is currently a major problem that impedes the development of nano-sized integrated optical circuits and other nano-optical applications. The main reason for this problem is the diffraction limit of light that does not allow localization of electromagnetic waves in regions noticeably smaller than half the effective wavelength in the structure [12–14]. One of the main directions to overcome this diffraction limit and achieving sub-diffraction limit localization is related to guided modes of surface plasma waves (plasmons) in metallic (negative dielectric permittivity) nano-sized structures. These include metallic nano-strips [15–18], nano-rods [14, 19], nano-chains [12, 13, 20, 21], gap-plasmons [22–25], channel plasmon-polaritons (CPPs) [26–30], etc.

✉ Fax: +81-88-656-8412,
E-mail: pile@opt.tokushima-u.ac.jp, d.pile@qut.edu.au

Therefore we present a compact-2D method that allows for negative cases of the dielectric permittivity (and magnetic permeability) by implementing the Drude model of the electric (and equivalent magnetic) charges in the compact-2D FDTD algorithm. While 3D FDTD methods have limitations on the waveguide geometries that can be analyzed, because of extensive computational resources required, the presented compact-2D FDTD method essentially removes this limitation, allowing analysis of practically any waveguide shape and any materials including those exhibiting positive dielectric permittivity, negative dielectric permittivity, negative magnetic permeability and negative refractive index. Also, we present the derivation of the FDTD algorithm given in [3, 4] extended to 3D and also allowing for negative magnetic permeability ([3, 4] gave only the 2D description and only allowing for negative dielectric permittivity).

2 3D formulation with electric and equivalent magnetic charges

We model the motion of electronic charges using the kinetic force equation as was done in [3, 4], and we extend to three dimensions and introduce equivalent magnetic charges (in addition to the electric charges). The current densities are introduced into the Maxwell equations as follows:

$$\frac{\partial \mathbf{B}}{\partial t} = -\nabla \times \mathbf{E} - \mathbf{J}_\mathrm{m} \tag{1}$$

Faraday's law and

$$\frac{\partial \mathbf{D}}{\partial t} = \nabla \times \mathbf{H} - \mathbf{J}_\mathrm{e} \tag{2}$$

Ampere's law. From Eqs. (1) and (2) we obtain

$$\begin{aligned}
\frac{\partial H_\mathrm{x}}{\partial t} &= \frac{1}{\mu}\left[\frac{\partial E_\mathrm{y}}{\partial z} - \frac{\partial E_\mathrm{z}}{\partial y} - J_{\mathrm{m,x}}\right] \\
\frac{\partial H_\mathrm{y}}{\partial t} &= \frac{1}{\mu}\left[\frac{\partial E_\mathrm{z}}{\partial x} - \frac{\partial E_\mathrm{x}}{\partial z} - J_{\mathrm{m,y}}\right] \\
\frac{\partial H_\mathrm{z}}{\partial t} &= \frac{1}{\mu}\left[\frac{\partial E_\mathrm{x}}{\partial y} - \frac{\partial E_\mathrm{y}}{\partial x} - J_{\mathrm{m,z}}\right] \\
\frac{\partial E_\mathrm{x}}{\partial t} &= \frac{1}{\varepsilon}\left[\frac{\partial H_\mathrm{z}}{\partial y} - \frac{\partial H_\mathrm{y}}{\partial z} - J_{\mathrm{e,x}}\right] \\
\frac{\partial E_\mathrm{y}}{\partial t} &= \frac{1}{\varepsilon}\left[\frac{\partial H_\mathrm{x}}{\partial z} - \frac{\partial H_\mathrm{z}}{\partial x} - J_{\mathrm{e,y}}\right] \\
\frac{\partial E_\mathrm{z}}{\partial t} &= \frac{1}{\varepsilon}\left[\frac{\partial H_\mathrm{y}}{\partial x} - \frac{\partial H_\mathrm{x}}{\partial y} - J_{\mathrm{e,z}}\right]
\end{aligned} \tag{3}$$

where ε and μ are the dielectric permittivity and magnetic permeability, that are assumed to be positive, while the response of the material due to charges is modeled in the electric and magnetic current densities, $\mathbf{J}_\mathrm{e}$ and $\mathbf{J}_\mathrm{m}$, i.e., charges are moving in the material that has positive ε and μ (e.g., charges in vacuum for the case for metals). Discretizing space and time by substituting the derivatives in Eq. (3) with central differences (that are second-order accurate [1]) using the Yee scheme [1, 2] illustrated in Fig. 1 we obtain

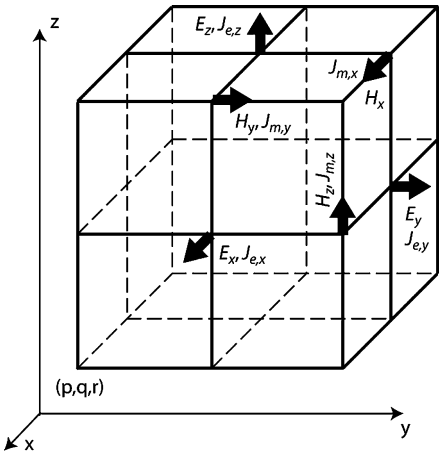

FIGURE 1 3D Yee unit cell showing the location at which each field component and current density is determined

$$\begin{aligned}
E_\mathrm{x}\big|^{\mathrm{n}+1/2}_{\mathrm{p,q}+1/2,\mathrm{r}+1/2} &= E_\mathrm{x}\big|^{\mathrm{n}-1/2}_{\mathrm{p,q}+1/2,\mathrm{r}+1/2} \\
&+ \frac{\Delta t}{\varepsilon_{\mathrm{p,q}+1/2,\mathrm{r}+1/2}}\left[\frac{H_\mathrm{z}\big|^{\mathrm{n}}_{\mathrm{p,q}+1,\mathrm{r}+1/2} - H_\mathrm{z}\big|^{\mathrm{n}}_{\mathrm{p,q,r}+1/2}}{\Delta y}\right. \\
&\left. - \frac{H_\mathrm{y}\big|^{\mathrm{n}}_{\mathrm{p,q}+1/2,\mathrm{r}+1} - H_\mathrm{y}\big|^{\mathrm{n}}_{\mathrm{p,q}+1/2,\mathrm{r}}}{\Delta z} - J_{\mathrm{e,x}}\big|^{\mathrm{n}}_{\mathrm{p,q}+1/2,\mathrm{r}+1/2}\right] \\
E_\mathrm{y}\big|^{\mathrm{n}+1/2}_{\mathrm{p}-1/2,\mathrm{q}+1,\mathrm{r}+1/2} &= E_\mathrm{y}\big|^{\mathrm{n}-1/2}_{\mathrm{p}-1/2,\mathrm{q}+1,r+1/2} \\
&+ \frac{\Delta t}{\varepsilon_{\mathrm{p}-1/2,q+1,r+1/2}}\left[\frac{H_\mathrm{x}\big|^{\mathrm{n}}_{\mathrm{p}-1/2,\mathrm{q}+1,\mathrm{r}+1} - H_\mathrm{x}\big|^{\mathrm{n}}_{\mathrm{p}-1/2,\mathrm{q}+1,\mathrm{r}}}{\Delta z}\right. \\
&- \frac{H_\mathrm{z}\big|^{\mathrm{n}}_{\mathrm{p,q}+1,\mathrm{r}+1/2} - H_\mathrm{z}\big|^{\mathrm{n}}_{\mathrm{p}-1,\mathrm{q}+1,\mathrm{r}+1/2}}{\Delta x} \\
&\left. - J_{\mathrm{e,y}}\big|^{\mathrm{n}}_{\mathrm{p}-1/2,\mathrm{q}+1,\mathrm{r}+1/2}\right] \\
E_\mathrm{z}\big|^{\mathrm{n}+1/2}_{\mathrm{p}-1/2,\mathrm{q}+1/2,\mathrm{r}+1} &= E_\mathrm{y}\big|^{\mathrm{n}-1/2}_{\mathrm{p}-1/2,\mathrm{q}+1/2,\mathrm{r}+1} + \frac{\Delta t}{\varepsilon_{\mathrm{p}-1/2,\mathrm{q}+1/2,\mathrm{r}+1}} \\
&\times \left[\frac{H_\mathrm{y}\big|^{\mathrm{n}}_{\mathrm{p,q}+1/2,\mathrm{r}+1} - H_\mathrm{y}\big|^{\mathrm{n}}_{\mathrm{p}-1,\mathrm{q}+1/2,\mathrm{r}+1}}{\Delta x}\right. \\
&- \frac{H_\mathrm{x}\big|^{\mathrm{n}}_{\mathrm{p}-1/2,\mathrm{q}+1,\mathrm{r}+1} - H_\mathrm{x}\big|^{\mathrm{n}}_{\mathrm{p}-1/2,\mathrm{q,r}+1}}{\Delta \mathrm{y}} \\
&\left. - J_{\mathrm{e,z}}\big|^{\mathrm{n}}_{\mathrm{p}-1/2,\mathrm{q}+1/2,\mathrm{r}+1}\right] \\
H_\mathrm{x}\big|^{\mathrm{n}+1}_{\mathrm{p}-1/2,\mathrm{q}+1,\mathrm{r}+1} &= H_\mathrm{x}\big|^{\mathrm{n}}_{\mathrm{p}-1/2,\mathrm{q}+1/2,\mathrm{r}+1} + \frac{\Delta t}{\mu_{\mathrm{p}-1/2,\mathrm{q}+1,\mathrm{r}+1}} \\
&\times \left[\frac{E_\mathrm{y}\big|^{\mathrm{n}+1/2}_{\mathrm{p}-1/2,\mathrm{q}+1,\mathrm{r}+3/2} - E_\mathrm{y}\big|^{\mathrm{n}+1/2}_{\mathrm{p}-1/2,\mathrm{q}+1,\mathrm{r}+1/2}}{\Delta z}\right. \\
&- \frac{E_\mathrm{z}\big|^{\mathrm{n}+1/2}_{\mathrm{p}-1/2,\mathrm{q}+3/2,\mathrm{r}+1} - E_\mathrm{z}\big|^{\mathrm{n}+1/2}_{\mathrm{p}-1/2,\mathrm{q}+1/2,\mathrm{r}+1}}{\Delta y}
\end{aligned}$$

$$- J_{m,x}\big|^{n+1/2}_{p-1/2,q+1,r+1}\Bigg]$$

$$H_y\big|^{n+1}_{p,q+1/2,r+1} = H_y\big|^{n}_{p,q+1/2,r+1} + \frac{\Delta t}{\mu_{p,q+1/2,r+1}} \times \Bigg[\frac{E_z\big|^{n+1/2}_{p+1/2,q+1/2,r+1} - E_z\big|^{n+1/2}_{p-1/2,q+1/2,r+1}}{\Delta x} - \frac{E_x\big|^{n+1/2}_{p,q+1/2,r+3/2} - E_x\big|^{n+1/2}_{p,q+1/2,r+1/2}}{\Delta z} - J_{m,y}\big|^{n+1/2}_{p,q+1/2,r+1}\Bigg]$$

$$H_z\big|^{n+1}_{p,q+1,r+1/2} = H_z\big|^{n}_{p,q+1,r+1/2} + \frac{\Delta t}{\mu_{p,q+1,r+1/2}} \times \Bigg[\frac{E_x\big|^{n+1/2}_{p,q+3/2,r+1/2} - E_x\big|^{n+1/2}_{p,q+1/2,r+1/2}}{\Delta y} - \frac{E_y\big|^{n+1/2}_{p+1/2,q+1,r+1/2} - E_y\big|^{n+1/2}_{p-1/2,q+1,r+1/2}}{\Delta x} - J_{m,z}\big|^{n+1/2}_{p,q+1,r+1/2}\Bigg] \tag{4}$$

where the p, q, r and n indices represent discrete coordinates in the x, y, z and t axes, respectively. The motion of the charges that give rise to the current densities $\mathbf{J}_e$ and $\mathbf{J}_m$ in Eq. (4) is determined using either a local bound electron or local Drude model as follows. The net force, $\mathbf{F}_{net}$, on a charge is taken as

$$\mathbf{F}_{net} = m\mathbf{a}_{net} = \mathbf{F}_{field} + \mathbf{F}_{damping} + \mathbf{F}_{restoring} \tag{5}$$

where $\mathbf{F}_{field}$ is force on a charge due to the presence of a field (electric field for electrons or magnetic field for equivalent magnetic charges), $\mathbf{F}_{damping}$ is the force that results in kinetic energy loss due to collisions (i.e., dissipation) and $\mathbf{F}_{restoring}$ is the restoring force on the charge due to any binding to a positively charged region (e.g., positive atomic core for the electron). $\mathbf{F}_{field} = q\mathbf{G}$, where q is the charge (electronic, or equivalent magnetic charge) and $\mathbf{G}$ is either the electric field, $\mathbf{E}$, for the case of electrons, or the magnetic field, $\mathbf{H}$, for equivalent magnetic charges. $\mathbf{F}_{damping} = -m\omega_d\mathbf{v} = -m\omega_d d\mathbf{r}/dt$, where m, ω_d, $\mathbf{v}$ and $\mathbf{r}$ are the charge mass, damping frequency, velocity and displacement respectively. $\mathbf{F}_{restoring} = -k\mathbf{r} = -m\omega_r^2\mathbf{r}$, where k is the effective spring constant on the charge related to its binding to a positively charged core. Therefore Eq. (5) can be written as

$$m\frac{\partial^2\mathbf{r}}{\partial t^2} = q\mathbf{G} - m\omega_d\frac{\partial\mathbf{r}}{\partial t} - m\omega_r^2\mathbf{r}$$

or

$$m\frac{\partial\mathbf{v}}{\partial t} = q\mathbf{G} - m\omega_d\frac{\partial\mathbf{r}}{\partial t} - m\omega_r^2\int_0^t \mathbf{v}\partial t. \tag{6}$$

The acceleration $\partial\mathbf{v}/\partial t$ is approximated by the finite difference,

$$\frac{\partial\mathbf{v}}{\partial t} \approx \frac{\mathbf{v}^{n+1/2} - \mathbf{v}^{n-1/2}}{\Delta t} \tag{7}$$

and the displacement (the integral of velocity with respect to time) is approximated by

$$\mathbf{r}^n = \int_0^t \vec{v}\partial t \approx \sum_{m=1}^{n}\mathbf{v}^{m-1/2}\Delta t \tag{8}$$

and the velocity, $\mathbf{v}$, is taken as

$$\mathbf{v} \approx \frac{v^{n+1/2} + v^{n-1/2}}{2}. \tag{9}$$

Using Eqs. (7)–(9) with Eq. (6) and rearranging gives

$$\mathbf{v}^{n+1/2} = \left(1 + \frac{\Delta t\omega_d}{2}\right)^{-1}\Bigg[\left(1 - \frac{\Delta t\omega_d}{2}\right)\mathbf{v}^{n-1/2} - \omega_r^2\Delta t^2\sum_{m=1}^{n}\mathbf{v}^{m-1/2} + \frac{q\Delta t}{m}\mathbf{G}^{n+1/2}\Bigg] \tag{10}$$

where it should be noted that time indices (superscript of $\mathbf{v}$ and $\mathbf{G}$) are given for the case of electrons in the electric field, but for the equivalent magnetic charges in the magnetic field, the indices are displaced by 1/2 (according to the staggering in time of the calculation of the magnetic field [1]). Various approximations of Eq. (10) can be made when the damping or restoring forces on the electric or magnetic charges are negligible. For example, in a dielectric at a frequency near an electronic resonance with negligible damping ($\omega_d \approx 0$), it is possible to describe the electron motion by

$$\mathbf{v}^{n+1/2} = \mathbf{v}^{n-1/2} - \omega_r^2\Delta t^2\sum_{m=1}^{n}\mathbf{v}^{m-1/2} + \frac{q\Delta t}{m}\mathbf{E}^{n+1/2}. \tag{11}$$

Alternatively, for a metal below the plasma frequency we can disregard the binding force on the electrons ($\omega_r \approx 0$) and the positive atomic cores giving,

$$\mathbf{v}^{n+1/2} = \left(1 + \frac{\Delta t\omega_d}{2}\right)^{-1} \times \left[\left(1 - \frac{\Delta t\omega_d}{2}\right)\mathbf{v}^{n-1/2} + \frac{q\Delta t}{m}\mathbf{E}^{n+1/2}\right] \tag{12}$$

which, after disregarding damping this simplifies to

$$\mathbf{v}^{n+1/2} = \mathbf{v}^{n-1/2} + \frac{q\Delta t}{m}\mathbf{E}^{n+1/2}. \tag{13}$$

The current densities required in Eq. (4) are then given by

$$J_{e,x}\big|^{n}_{p,q+1/2,r+1/2} = \rho_e\ v_{e,x}\big|^{n-1/2}_{p,q+1/2,r+1/2}$$

$$J_{e,y}\big|^{n}_{p-1/2,q+1,r+1/2} = \rho_e\ v_{e,y}\big|^{n-1/2}_{p-1/2,q+1,r+1/2}$$

$$J_{e,z}\big|^{n}_{p-1/2,q+1/2,r+1} = \rho_e\ v_{e,z}\big|^{n-1/2}_{p-1/2,q+1/2,r+1}$$

$$J_{m,x}\big|^{n+1/2}_{p-1/2,q+1,r+1} = \rho_m\ v_{m,x}\big|^{n}_{p-1/2,q+1,r+1}$$

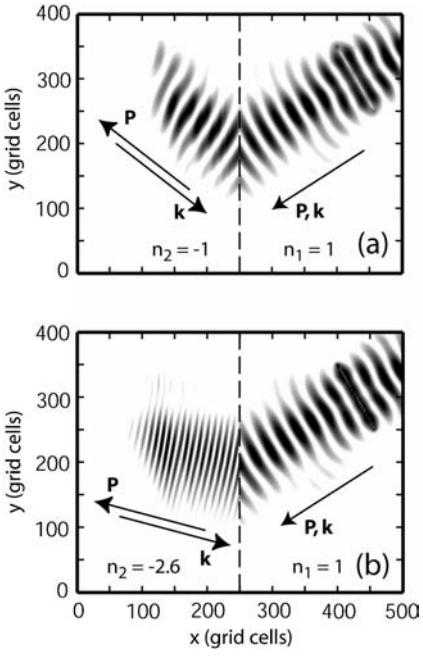

FIGURE 2 The electric field of an incident beam undergoing negative refraction. The EM wave is incident from the right (in a vacuum, i.e., $n_1 = 1$). **a** Negative refraction for the case of $|n_2| = |n_1| = 1$. **b** Negative refraction for the case of $|n_2| > |n_1|$

$$J_{\mathrm{m,y}}\big|^{\mathrm{n+1/2}}_{\mathrm{p,q+1/2,r+1}} = \rho_{\mathrm{m}}\ v_{\mathrm{m,y}}\big|^{\mathrm{n}}_{\mathrm{p,q+1/2,r+1}}$$
$$J_{\mathrm{m,z}}\big|^{\mathrm{n+1/2}}_{\mathrm{p,q+1,r+1/2}} = \rho_{\mathrm{m}}\ v_{\mathrm{m,z}}\big|^{\mathrm{n}}_{\mathrm{p,q+1,r+1/2}} \qquad (14)$$

where ρ_{e} and ρ_{m} are the electron and magnetic charge densities, respectively and $v_{\mathrm{e,x,y,z}}$ and $v_{\mathrm{m,x,y,z}}$ are respectively the velocity of electrons and magnetic charges as determined by Eq. (10) (or a further approximation of Eq. (10), e.g. Eq. (11)–(13)).

As a numerical example we give a demonstration of refraction at an interface between two materials: one that has positive dielectric permittivity and permeability (positive refractive index) and one that has negative dielectric permittivity and magnetic permeability (negative refractive index). In this case we can reduce the 3D FDTD equations to the 2D case (we assumed that the field is homogenous along the z-axis). Figure 2 shows the electric field distribution, $|E|$, some time after the incident wave in the material with positive refractive index reaches (from the right hand side) the interface at $x = 250$ (cells). In the time-domain results the phase fronts of the beam in the negative refractive index material were observed to be moving in the opposite direction to the direction of energy flow into the material (as indicated by directions of the wavevector **k** and Poynting vector **P** (Fig. 2)). The negative angles of refraction in the material with negative refractive index, θ_2, are the same (within the uncertainty of the numerical results) as determined from Snell's law, $n_1 \sin\theta_1 = n_2 \sin\theta_2$ taking n_1 and θ_1 as positive and n_2 as negative. Also, the decreased wavelength in the negative refractive index material with $n_2 > n_1$ (Fig. 2b, $x < 250$) is given by $\lambda_2 = \lambda_{\mathrm{vac}}/|n_2|$. These results are in agreement with previous results for negative refractive index materials [5, 6, 8, 31].

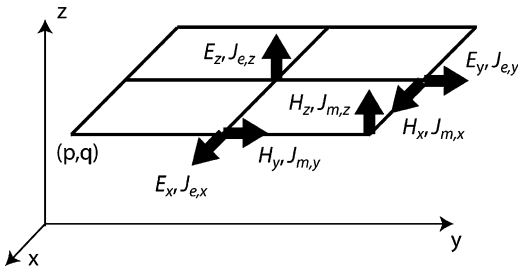

FIGURE 3 Compact-2D unit cell showing the location at which each field component is determined. The grid is obtained by taking the 3D grid (Fig. 1) in the limit $\Delta z \to 0$

3 Compact-2D formulation with electric and magnetic charges

Here we extend the compact-2D formulation derived previously for dielectric waveguide structures with positive dielectric permittivity [9–11] to enable simulation with materials that can also possess negative dielectric permittivity, negative magnetic permeability or any combinations of such materials (i.e., negative refractive index materials). We assume translational symmetry of the structure along the direction of propagation (z axis) and that the wave number of the guided mode is given by k. Therefore every field component of the guided mode has the form $G(x, y, z) = G(x, y)\exp(ikz)$ (where here, $i = (-1)^{1/2}$). In this case if we calculate the field components at one z-coordinate, we automatically know them everywhere and further, we do not need to numerically approximate the derivatives of the fields with respect to the z axis since we can get them analytically given the assumed form of the fields, i.e., the 3D guided-mode problem is reduced to a 2D problem. Figure 3 gives the 2D grid which is equivalent to the 3D grid in Fig. 1 but compressed in the z axis (i.e., we take the limit $\Delta z \to 0$). Taking the Maxwell Eqs. (1) and (2) and repeating the derivation in a similar fashion to Sect. 2 but using the assumed form of the field gives

$$E_{\mathrm{x}}\big|^{\mathrm{n+1/2}}_{\mathrm{p,q+1/2}} = E_{\mathrm{x}}\big|^{\mathrm{n-1/2}}_{\mathrm{p,q+1/2}} + \frac{\Delta t}{\varepsilon_{\mathrm{p,q+1/2}}} \times \left[\frac{H_{\mathrm{z}}\big|^{\mathrm{n}}_{\mathrm{p,q+1}} - H_{\mathrm{z}}\big|^{\mathrm{n}}_{\mathrm{p,q}}}{\Delta y} - ikH_{\mathrm{y}}\big|^{\mathrm{n}}_{\mathrm{p,q+1/2}} - J_{\mathrm{e,x}}\big|^{\mathrm{n}}_{\mathrm{p,q+1/2}}\right]$$

$$E_{\mathrm{y}}\big|^{\mathrm{n+1/2}}_{\mathrm{p-1/2,q+1}} = E_{\mathrm{y}}\big|^{\mathrm{n-1/2}}_{\mathrm{p-1/2,q+1}} + \frac{\Delta t}{\varepsilon_{\mathrm{p-1/2,q+1}}}\left[ikH_{\mathrm{x}}\big|^{\mathrm{n}}_{\mathrm{p-1/2,q+1}} - \frac{H_{\mathrm{z}}\big|^{\mathrm{n}}_{\mathrm{p,q+1}} - H_{\mathrm{z}}\big|^{\mathrm{n}}_{\mathrm{p-1,q+1}}}{\Delta x} - J_{\mathrm{e,y}}\big|^{\mathrm{n}}_{\mathrm{p-1/2,q+1}}\right]$$

$$E_{\mathrm{z}}\big|^{\mathrm{n+1/2}}_{\mathrm{p-1/2,q+1/2}} = E_{\mathrm{z}}\big|^{\mathrm{n-1/2}}_{\mathrm{p-1/2,q+1/2}} + \frac{\Delta t}{\varepsilon_{\mathrm{p-1/2,q+1/2}}}\left[\frac{H_{\mathrm{y}}\big|^{\mathrm{n}}_{\mathrm{p,q+1/2}} - H_{\mathrm{y}}\big|^{\mathrm{n}}_{\mathrm{p-1,q+1/2}}}{\Delta x} - \frac{H_{\mathrm{x}}\big|^{\mathrm{n}}_{\mathrm{p-1/2,q+1}} - H_{\mathrm{x}}\big|^{\mathrm{n}}_{\mathrm{p-1/2,q}}}{\Delta y} - J_{\mathrm{e,z}}\big|^{\mathrm{n}}_{\mathrm{p-1/2,q+1/2}}\right]$$

$$
\begin{aligned}
H_{\mathrm{x}}|^{\mathrm{n+1}}_{\mathrm{p-1/2,q+1}} &= H_{\mathrm{x}}|^{\mathrm{n}}_{\mathrm{p-1/2,q+1/2}} \\
&+ \frac{\Delta t}{\mu_{\mathrm{p-1/2,q+1}}}\left[ikE_{\mathrm{y}}|^{\mathrm{n+1/2}}_{\mathrm{p-1/2,q+1}} \right. \\
&\left. - \frac{E_{\mathrm{z}}|^{\mathrm{n+1/2}}_{\mathrm{p-1/2,q+3/2}} - E_{\mathrm{z}}|^{\mathrm{n+1/2}}_{\mathrm{p-1/2,q+1/2}}}{\Delta y} - J_{\mathrm{m,x}}|^{\mathrm{n+1/2}}_{\mathrm{p-1/2,q+1}} \right] \\
H_{\mathrm{y}}|^{\mathrm{n+1}}_{\mathrm{p,q+1/2}} &= H_{\mathrm{y}}|^{\mathrm{n}}_{\mathrm{p,q+1/2}} \\
&+ \frac{\Delta t}{\mu_{\mathrm{p,q+1/2}}}\left[\frac{E_{\mathrm{z}}|^{\mathrm{n+1/2}}_{\mathrm{p+1/2,q+1/2}} - E_{\mathrm{z}}|^{\mathrm{n+1/2}}_{\mathrm{p-1/2,q+1/2}}}{\Delta x} \right. \\
&\left. - ikE_{\mathrm{x}}|^{\mathrm{n+1/2}}_{\mathrm{p,q+1}} - J_{\mathrm{m,y}}|^{\mathrm{n+1/2}}_{\mathrm{p,q+1/2}} \right] \\
H_{\mathrm{z}}|^{\mathrm{n+1}}_{\mathrm{p,q+1}} &= H_{\mathrm{z}}|^{\mathrm{n}}_{\mathrm{p,q+1}} \\
&+ \frac{\Delta t}{\mu_{\mathrm{p,q+1}}}\left[\frac{E_{\mathrm{x}}|^{\mathrm{n+1/2}}_{\mathrm{p,q+3/2}} - E_{\mathrm{x}}|^{\mathrm{n+1/2}}_{\mathrm{p,q+1/2}}}{\Delta y} \right. \\
&\left. - \frac{E_{\mathrm{y}}|^{\mathrm{n+1/2}}_{\mathrm{p+1/2,q+1}} - E_{\mathrm{y}}|^{\mathrm{n+1/2}}_{\mathrm{p-1/2,q+1}}}{\Delta x} - J_{\mathrm{m,z}}|^{\mathrm{n+1/2}}_{\mathrm{p,q+1}} \right]
\end{aligned} \tag{15}
$$

where $\mathbf{J}_{\mathrm{e}}$ and $\mathbf{J}_{\mathrm{m}}$ are given by

$$
\begin{aligned}
J_{\mathrm{e,x}}|^{\mathrm{n}}_{\mathrm{p,q+1/2}} &= \rho_{\mathrm{e}}\ v_{\mathrm{e,x}}|^{\mathrm{n-1/2}}_{\mathrm{p,q+1/2}} \\
J_{\mathrm{e,y}}|^{\mathrm{n}}_{\mathrm{p-1/2,q+1}} &= \rho_{\mathrm{e}}\ v_{\mathrm{e,y}}|^{\mathrm{n-1/2}}_{\mathrm{p-1/2,q+1}} \\
J_{\mathrm{e,z}}|^{\mathrm{n}}_{\mathrm{i-1/2,j+1/2}} &= \rho_{\mathrm{e}}\ v_{\mathrm{e,z}}|^{\mathrm{n-1/2}}_{\mathrm{i-1/2,j+1/2}} \\
J_{\mathrm{m,x}}|^{\mathrm{n+1/2}}_{\mathrm{i-1/2,j+1}} &= \rho_{\mathrm{m}}\ v_{\mathrm{m,x}}|^{\mathrm{n}}_{\mathrm{i-1/2,j+1}} \\
J_{\mathrm{m,y}}|^{\mathrm{n+1/2}}_{\mathrm{p,q+1/2}} &= \rho_{\mathrm{m}}\ v_{\mathrm{m,y}}|^{\mathrm{n}}_{\mathrm{p,q+1/2}} \\
J_{\mathrm{m,z}}|^{\mathrm{n+1/2}}_{\mathrm{p,q+1}} &= \rho_{\mathrm{m}}\ v_{\mathrm{m,z}}|^{\mathrm{n}}_{\mathrm{p,q+1}}
\end{aligned} \tag{16}
$$

where $\mathbf{v}$ are given by Eq. (10) or the further approximations (Eqs. (11)–(13)). The stability condition for the size of the time step Δt in the compact-2D FDTD scheme was obtained previously [10] as

$$
\Delta t_{\max} \le \frac{1}{v}\left[\frac{1}{\Delta x^2} + \frac{1}{\Delta y^2} + \left(\frac{k}{2}\right)^2 \right]^{-1/2} \tag{17}
$$

where v is the speed of light in the considered materials (not in a vacuum as reported in [11]). Eq. (15) introduces complex numbers that pose no problem other than increased computation time. It is possible to get rid of the complex numbers by assuming instead of $G(x, y, z) = G(x, y)\exp(ikz)$, that E_{z}, H_{x}, H_{y}, have $\cos(kz + \phi)$ forms and H_{z}, E_{x}, E_{y} have $\sin(kz + \phi)$ [11, 32] forms giving, instead of Eq. (15),

$$
\begin{aligned}
E_{\mathrm{x}}|^{\mathrm{n+1/2}}_{\mathrm{p,q+1/2}} &= E_{\mathrm{x}}|^{\mathrm{n-1/2}}_{\mathrm{p,q+1/2}} + \frac{\Delta t}{\varepsilon_{\mathrm{p,q+1/2}}} \\
&\times \left[\frac{H_{\mathrm{z}}|^{\mathrm{n}}_{\mathrm{p,q+1}} - H_{\mathrm{z}}|^{\mathrm{n}}_{\mathrm{p,q}}}{\Delta y} + kH_{\mathrm{y}}|^{\mathrm{n}}_{\mathrm{p,q+1/2}} - J_{\mathrm{e,x}}|^{\mathrm{n}}_{\mathrm{p,q+1/2}} \right] \\
E_{\mathrm{y}}|^{\mathrm{n+1/2}}_{\mathrm{p-1/2,q+1}} &= E_{\mathrm{y}}|^{\mathrm{n-1/2}}_{\mathrm{p-1/2,q+1}} \\
&+ \frac{\Delta t}{\varepsilon_{\mathrm{p-1/2,q+1}}}\left[-kH_{\mathrm{x}}|^{\mathrm{n}}_{\mathrm{p-1/2,q+1}} - \frac{H_{\mathrm{z}}|^{\mathrm{n}}_{\mathrm{p,q+1}} - H_{\mathrm{z}}|^{\mathrm{n}}_{\mathrm{p-1,q+1}}}{\Delta x} \right. \\
&\left. - J_{\mathrm{e,y}}|^{\mathrm{n}}_{\mathrm{p-1/2,q+1}} \right] \\
E_{\mathrm{z}}|^{\mathrm{n+1/2}}_{\mathrm{p-1/2,q+1/2}} &= E_{\mathrm{z}}|^{\mathrm{n-1/2}}_{\mathrm{p-1/2,q+1/2}} + \frac{\Delta t}{\varepsilon_{\mathrm{p-1/2,q+1/2}}} \\
&\times \left[\frac{H_{\mathrm{y}}|^{\mathrm{n}}_{\mathrm{p,q+1/2}} - H_{\mathrm{y}}|^{\mathrm{n}}_{\mathrm{p-1,q+1/2}}}{\Delta x} \right. \\
&\left. - \frac{H_{\mathrm{x}}|^{\mathrm{n}}_{\mathrm{p-1/2,q+1}} - H_{\mathrm{x}}|^{\mathrm{n}}_{\mathrm{p-1/2,q}}}{\Delta y} - J_{\mathrm{e,z}}|^{\mathrm{n}}_{\mathrm{p-1/2,q+1/2}} \right] \\
H_{\mathrm{x}}|^{\mathrm{n+1}}_{\mathrm{p-1/2,q+1}} &= H_{\mathrm{x}}|^{\mathrm{n}}_{\mathrm{p-1/2,q+1/2}} \\
&+ \frac{\Delta t}{\mu_{\mathrm{p-1/2,q+1}}}\left[kE_{\mathrm{y}}|^{\mathrm{n+1/2}}_{\mathrm{p-1/2,q+1}} \right. \\
&\left. - \frac{E_{\mathrm{z}}|^{\mathrm{n+1/2}}_{\mathrm{p-1/2,q+3/2}} - E_{\mathrm{z}}|^{\mathrm{n+1/2}}_{\mathrm{p-1/2,q+1/2}}}{\Delta y} - J_{\mathrm{m,x}}|^{\mathrm{n+1/2}}_{\mathrm{p-1/2,q+1}} \right] \\
H_{\mathrm{y}}|^{\mathrm{n+1}}_{\mathrm{p,q+1/2}} &= H_{\mathrm{y}}|^{\mathrm{n}}_{\mathrm{p,q+1/2}} \\
&+ \frac{\Delta t}{\mu_{\mathrm{p,q+1/2}}}\left[\frac{E_{\mathrm{z}}|^{\mathrm{n+1/2}}_{\mathrm{p+1/2,q+1/2}} - E_{\mathrm{z}}|^{\mathrm{n+1/2}}_{\mathrm{p-1/2,q+1/2}}}{\Delta x} \right. \\
&\left. - kE_{\mathrm{x}}|^{\mathrm{n+1/2}}_{\mathrm{p,q+1}} - J_{\mathrm{m,y}}|^{\mathrm{n+1/2}}_{\mathrm{p,q+1/2}} \right] \\
H_{\mathrm{z}}|^{\mathrm{n+1}}_{\mathrm{p,q+1}} &= H_{\mathrm{z}}|^{\mathrm{n}}_{\mathrm{p,q+1}} \\
&+ \frac{\Delta t}{\mu_{\mathrm{p,q+1}}}\left[\frac{E_{\mathrm{x}}|^{\mathrm{n+1/2}}_{\mathrm{p,q+3/2}} - E_{\mathrm{x}}|^{\mathrm{n+1/2}}_{\mathrm{p,q+1/2}}}{\Delta y} \right. \\
&\left. - \frac{E_{\mathrm{y}}|^{\mathrm{n+1/2}}_{\mathrm{p+1/2,q+1}} - E_{\mathrm{y}}|^{\mathrm{n+1/2}}_{\mathrm{p-1/2,q+1}}}{\Delta x} - J_{\mathrm{m,z}}|^{\mathrm{n+1/2}}_{\mathrm{p,q+1}} \right].
\end{aligned} \tag{18}
$$

As a demonstration, CPPs guided by a triangular metal groove [27–30] are considered. A CPP waveguide makes a good test example because of the rapidly changing fields (in space) and the presence of a sharp point in the structure making numerical simulation challenging (time consuming or impossible for some groove angles using the 3D FDTD method [27–30]). The waveguide structure is presented in Fig. 4a. Artificial absorbing boundary conditions of the first-order Mur type are used at the edges of the computation window [33]. An initial field distribution is inserted into the computational window and the fields are iterated in the time domain. The initial field distribution should be pulsed in such a fashion as to include any desired frequencies of interest. After sufficient time iteration the non-physical fields vanish and only physical field components (steady state and time harmonic) linger, if any exist for the considered structure (at the assumed wave number, within the range of frequencies excited). In the presented calculations the time dependence of the incident pulse

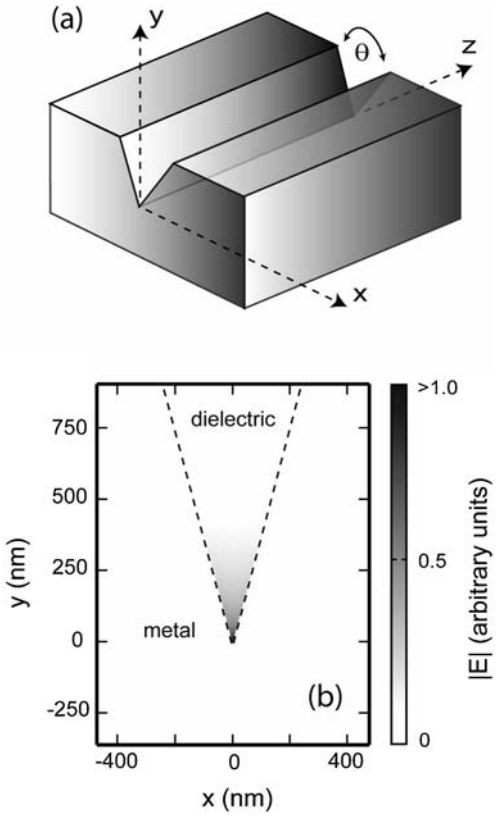

FIGURE 4 **a** The structure with a triangular groove in a metal substrate. **b** Distribution of the magnitude of the electric field in the vacuum groove ($\varepsilon = 1$) in silver with free charge density $\rho_e = -7.684 \times 10^9$ C/m^{-3} ($\rho_m = 0$) and damping frequency $f_d = 0$ (giving $\varepsilon_m = -16.22$) after 20000 time iterations. Groove angle is $\theta = 30^\circ$ and $k = 1.2 \times 10^7$ m^{-1}

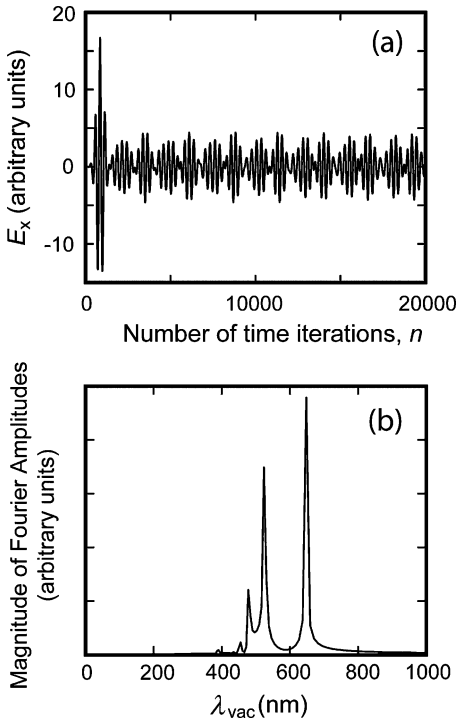

FIGURE 5 **a** Amplitude of E_x at tip of the groove versus time ($t = n\Delta t = n \times 0.95\Delta t_{max}$). The incident pulse can be seen in the region $n < 2000$. Groove angle $\theta = 10^\circ$ and $k = 1.7 \times 10^7$ m^{-1}. **b** Dependence of the Fourier amplitude of the field at the tip of the groove (Fig. 5a, taking $n > 2000$) on the wavelength in a vacuum

is given by

$$\mathbf{E}|^{n+1/2} = \mathbf{E}|^{n-1/2} + E_0 \sin\{\omega_0(n - n_{delay})\Delta t\} \times \exp\left\{-\frac{(n - n_{delay})^2}{\tau^2}\right\} \quad (19)$$

where ω_0 is the central frequency of the pulse. In the present examples, $\lambda_{vac} = 632.8$ nm, $n_{delay} = 3\tau$, $\tau = 2 \times 10^{-15}/\Delta t$, $\Delta t = 0.95\Delta t_{max}$ (determined with Eq. (17), given $\Delta x, y = \lambda_{vac}/400$ for the data presented below). The more similar the initial field distribution is to that of the eigenmodes (if they exist) then the less number of time-itterations will be required to achieve the steady-state result. However, the initial field distribution need not be that similar to that of the desired guided mode if computation time is sacrificed slightly (due to an increased number of iterations required to reach the steady-state situation). Therefore the initial field distribution is not that critical since the presented method is highly efficient. For example, for the excitation of the CPP waveguide whose guided mode is expected to be strongly localized to the tip of the channel, it is sufficient to introduce the incident source at only the single grid cell at the tip of the groove (as was done for the data presented below). On the other hand, the polarization of the incident field is critical and the incident source should share at least one field component with that of the guided mode.

Figure 4b shows the resultant steady-state electric field distribution in the cross-section of waveguide and we can see a highly localized plasmon guided mode at the apex of the groove that is exponentially decaying in the both the y and x directions from the apex but propagating in the z direction. The field distribution is in good agreement with that obtained from the 3D method [27–30]. To obtain this result using the compact-2D method requires 2 hours of computation time using a 2Ghz CPU compared to about 2 days for the 3D method (and can not even be calculated using a conventional PC with the similarly small grid cell size (and hence accuracy)). In addition, while calculating the same cross-sectional area of the waveguide with the same grid spacing the compact-2D method requires about $z_{total}/\Delta z$ times less memory than the 3D method, where z_{total} is the length of the computation window in the direction of propagation. E.g. if a $z_{total} \sim 5\lambda_{vac}$ is required to achieve the steady state guided mode free of interference from the incident beam, etc., then taking $\Delta z = \lambda_{vac}/50$ (which is likely to be insufficient for many structures) we will use about 250 times more memory using the 3D method than in the compact-2D method. Hence the compact-2D method will be immediately applicable to a much wider range of structures than the 3D method.

When we introduce the field into the waveguide, we automatically generate all modes (that are resolved with the used grid resolution and in the range of frequencies contained in the incident pulse) that have the assumed propagation constant, k. Therefore, in the structure that supports multiple modes

at the given propagation constant, the field in the waveguide will experience beats in time due to the interference of the co-propagating modes that oscillate with different frequency. This interference is evident in Fig. 5a that shows the typical time dependence of the field at the tip of the CPP waveguide. In Fig. 5a we can also see the shape and duration of the incident pulse ($n <\sim 2000$) and that a steady-state has clearly been achieved.

The time-domain field at the tip of the groove (Fig. 5a, $n > 2000$ (to avoid the incident pulse)) is converted to the frequency domain by expanding the field into the Fourier integral and the Fourier amplitudes are expressed as a function of wavelength in a vacuum (or equivalently, frequency) – see Fig. 5b. The maxima correspond to frequencies at which the guided modes exist in the structure with the assumed propagation constant, $k = 1.7 \times 10^7$ m^{-1} (the righter-most peak corresponds the fundamental mode). It should be noted that using either the complex (Eq. (15)) or real (Eq. (18)) did not give any change in eigen-frequencies for the considered structure.

4 Conclusions

A 3D description of the FDTD algorithm for bound and free electronic and equivalent magnetic charges was given and an example of negative refraction illustrated the method. We presented a highly efficient compact-2D FDTD method for the analysis of waveguides that may include metallic, magnetic or negative refractive index materials. The method was demonstrated for the analysis of CPP guided modes in triangular grooves on a metal surface. Both a complex variable and real variable scheme were presented though no difference in the calculated eigen-frequencies was observed for the considered structure, although the real variable method was significantly faster (about 1/5). Computation time and memory compared to the three-dimensional calculations are drastically reduced, >100 times for typical problems. The computational savings, especially in terms of required memory, means that the presented method is applicable to the accurate analysis of range of waveguide structures that can not be considered using 3D-FDTD (or analytical methods).

REFERENCES

1 A. Taflove, S.C. Hagness, *Computational Electrodynamics*, 2nd edn. (Boston, Artech House 2000)
2 K.S. Yee, IEEE Trans. Antennas Propagat. **14**, 302 (1966)
3 D. Christensen, D. Fowers, Biosens. Bioelectron. **11**, 667 (1996)
4 D. Fowers, Masters Thesis (University of Utah, Salt Lake City, Utah, 1994)
5 V.G. Veselago, Soviet Phys. Uspekhi. **10**, 509 (1968)
6 R.A. Shelby, D.R. Smith, S. Schultz, Science. **292**, 77 (2001)
7 V.A. Podolskiy, A.K. Sarychev, V.M. Shalaev, Optics Express. **11**, 735 (2004)
8 R.W. Ziolkowski, Phys. Rev. E. **64**, 056625 (2001)
9 A. Asi, L. Shafai, Electron. Lett. **28**, 1451 (1992)
10 A. Cangellaris, IEEE Microwave and Guided Wave Lett. **3**, 3 (1993)
11 M. Qui, Microwave and Opt. Tech. Lett. **30**, 327 (2001)
12 J.R. Krenn, Nature Mater. **2**, 210 (2003)
13 S.A. Maier, P.G. Kik, H.A. Atwater, S. Meltzer, E. Harel, B.E. Koel, A.A.G. Requicha, Nature Mater. **2**, 229 (2003)
14 J. Takahara, S. Yamagishi, H. Taki, A. Morimoto, T. Kobayashi, Opt. Lett. **22**, 475 (1997)
15 P. Berini, Phys. Rev. B. **63**, 125417 (2001)
16 B. Lamprecht, J.R. Krenn, G. Schider, H. Ditlbacher, M. Salerno, N. Felidj, A. Leitner, F.R. Aussnegg, Appl. Phys. Lett. **79**, 51 (2001)
17 G. Schider, J.R. Krenn, A. Hohenau, H. Ditlbacher, A. Leitner, F.R. Aussenegg, W.L. Schaich, I. Puscasu, B. Monacelli, G. Boreman, Phys. Rev. B. **68**, 155427 (2003)
18 J.R. Krenn, B. Lamprecht, H. Ditlbacher, G. Schider, M. Salerno, A. Leitner, F.R. Aussenegg, Europhys. Lett. **663**, 663 (2002)
19 C.A. Pfeiffer, E.N. Economou, K.L. Ngai, Phys. Rev. B **10**, 3038 (1974)
20 J.R. Krenn, A. Dereux, J.C. Weeber, E. Bourillot, Y. Lacroute, J.P. Goudonnet, G. Schider, W. Gotschy, A. Leitner, F.R. Aussenegg, C. Girard, Phys. Rev. Lett. **82**, 2590 (1999)
21 S.A. Maier, M.L. Brongersma, H.A. Atwater, Appl. Phys. Lett. **78**, 16 (2001)
22 K. Tananka, M. Tanaka, Appl. Phys. Lett. **82**, 1158 (2003)
23 K. Tananka, M. Tanaka, T. Sugiyama, Optics Express. **13**, 256 (2005)
24 B. Wang, G.P. Wang, Appl. Phys. Lett. **85**, 3599 (2004)
25 B. Wang, G.P. Wang, Opt. Lett. **29**, 1992 (2004)
26 I.V. Novikov, A.A. Maradudin, Phys. Rev. B. **66**, 035403 (2002)
27 D.F.P. Pile, D.K. Gramotnev, Opt. Lett. **29**, 1069 (2004)
28 D.K. Gramotnev, D.F.P. Pile, Appl. Phys. Lett. **85**, 6323 (2004)
29 D.F.P. Pile, D.K. Gramotnev, Opt. Lett. **30**, 1186, (2005)
30 D.F.P. Pile, D.K. Gramotnev, Appl. Phys. Lett. **86**, 161101 (2005)
31 S. Foteinopoulou, E.N. Economou, C.M. Soukoulis, Phys. Rev. Lett. **90**, 107402 (2003)
32 M. Celuch-Marcysiak, W.K. Gwarek, IEEE Trans. Microwave Theory Tech. **43**, 860 (1995)
33 G. Mur, IEEE Trans. Electromagn. Compat. **40**, 100 (1998)